

Magnon and phonon assisted tunneling in a high-magnetoresistance tunnel junction using Co₇₅Fe₂₅ ferromagnetic electrodes

C. Lü,^{1,2} M. W. Wu,^{1,2,*} and X. F. Han³

¹Structure Research Laboratory, University of Science & Technology of China, Academia Sinica, Hefei, Anhui, 230026, China

²Department of Physics, University of Science & Technology of China, Hefei, Anhui, 230026, China[†]

³State Key Laboratory of Magnetism, Institute of Physics, Chinese Academy of Sciences, P.O. Box 603, Beijing 100080, China

(Dated: November 26, 2018)

Magnetolectric properties of the spin-valve-type tunnel junction of Ta(5 nm)/Ni₇₉Fe₂₁ (25 nm)/Ir₂₂Mn₇₈ (10 nm)/Co₇₅Fe₂₅ (4 nm)/Al (0.8 nm)-oxide/Co₇₅Fe₂₅ (4 nm)/Ni₇₉Fe₂₁ (20 nm)/Ta (5 nm) are investigated both experimentally and theoretically. It is shown that both magnon and phonon excitations contribute to the tunneling process. Moreover, we show that there are two branches of magnon with spin $S = 1/2$ and $3/2$ respectively. The theoretical results are in good agreement with the experimental data.

Tremendous interest has been devoted to the tunnel magnetoresistance (TMR) effect^{1,2,3,4,5,6,7,8,9,10} due to the high application potential in magnetic random access memory (MRAM) and magnetic-read-head technology.^{7,11,12,13,14} Spin-electron transport and nanoscale magnetism in ferromagnet/insulator/ferromagnet (FM/I/FM) junction structure play a very important role in this effect. Up to present, although considerable progress on both experimental and theoretical studies of TMR effect in FM/I/FM junctions has been achieved, intrinsic magnetolectric properties of magnetic tunnel junctions (MTJs) as well as spin-electron transport theory have not yet been generally reported. Therefore, a close study of these subjects are important both for the sake of fundamental studies and for the development of high-quality TMR devices.

Recently Han *et al.* performed a systematic experimental investigation of a spin-valve-type tunnel junction of Ta(5 nm)/Ni₇₉Fe₂₁ (3 nm)/Cu (20 nm)/Ni₇₉Fe₂₁ (3 nm)/Ir₂₂Mn₇₈ (10 nm)/Co₇₅Fe₂₅ (4 nm)/Al (0.8 nm)-oxide/Co₇₅Fe₂₅ (4 nm)/Ni₇₉Fe₂₁ (20 nm)/Ta (5 nm) by measuring the tunnel current I , dynamic conductance dI/dV and inelastic electron tunneling (IET) spectrum dG/dV ($G = I/V$) as functions of dc bias voltage V for both parallel (P) and antiparallel (AP) alignments of the magnetization of the two FM electrodes.¹⁰ By applying the magnon-assisted tunneling theory developed by Zhang *et al.*⁴ they fit their I - V , TMR- V , and TMR- T curves with a $S = 3/2$ magnon excitation $\omega_{\mathbf{q}} = E_m(q/q_m)^2$ for cut-off energy $E_m = 121$ meV and $q_m = \sqrt{4\pi n}$ where n is the density of atoms at an interface. However, there is more interesting information in their IET spectrum data which has not been fully discussed. In particular, the contribution of phonon-assisted tunneling to the tunneling current has not been accounted in their model and calculations.^{4,10} As shown in Fig. 1 there are three peaks in the IET spectrum from a new sample obtained in this work for $V > 0$ (or < 0): a strong peak around 20 meV and two small peaks around 90 and 115 meV. The small peak around 121 meV cor-

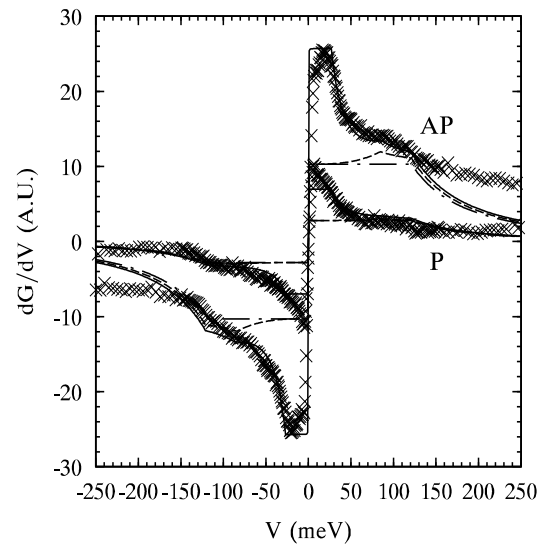


FIG. 1: IET spectrum via the single-magnon-assisted tunneling (dash-dotted curve), single-magnon and phonon-assisted tunneling (dashed curve) and double-magnon and single-phonon-assisted tunneling (solid curve) are plotted as functions of voltage V . The experimental data are plotted as crosses. $T = 4.2$ K.

respond to E_m of the magnon excitation. Another small peak around 90 meV is identified to be the phonon excitation in Al₂O₃ by Han *et al.* but has not been analyzed theoretically. The strong peak around 20 meV has not been clearly specified.

In this letter we combine both magnon-assisted tunneling theory developed by Zhang *et al.*⁴ and the phonon-assisted tunneling theory developed by Bratkovsky^{6,15} into one theory to analyze the experimental data obtained in this work. This is because that the intrinsic magnetolectric properties of an MTJ at nonzero bias voltages are closely related with the inelastic scattering in the tunneling progress for the conduction electrons. Ex-

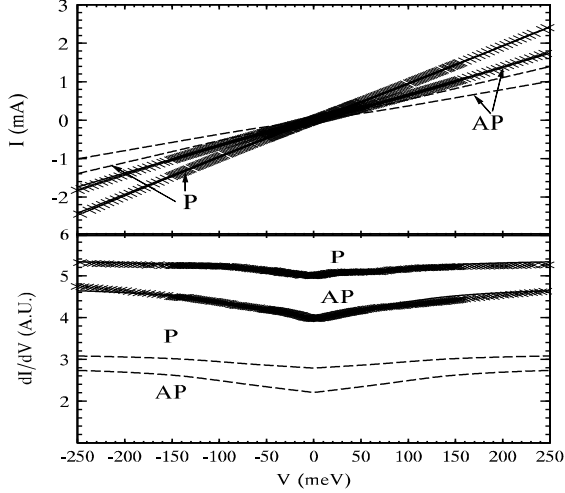


FIG. 2: Tunnel current I and dynamic conductance dI/dV versus bias voltage. Cross: Experimental data; Solid curve: Theoretical results of double-magnon and single-phonon assisted tunneling; Dashed curve: Theoretical results of single-magnon and single-phonon assisted tunneling. $T = 4.2$ K.

perimental results show that the coexisting magnon and phonon excitations are the main sources of the inelastic scattering in an MTJ,⁹ especially when the defects in the Al-O barrier and at the interfaces between FM/I/FM layers can be neglected for a good quality MTJ with very high-magnetoresistance and low resistance.⁸ Therefore, using a magnon- and phonon-assisted tunneling theory to evaluate the properties of an MTJ at elevated temperature or/and at nonzero bias voltages can achieve the desired and novel results.

In order to keep the same value of the intrinsic parameters mentioned below for calculating self-consistently the magnetoelectric properties of an MTJ using following formulas deduced in this work, it is necessary to use the same MTJ for all the experimental data measurement. Therefore, a series of experimental data was measured for a spin-valve-type MTJ of Ta (5 nm)/Ni₇₉Fe₂₁(25 nm)/Ir₂₂Mn₇₈(12 nm)/Co₇₅Fe₂₅(4 nm)/Al(0.8 nm)-oxide/Co₇₅Fe₂₅(4 nm)/Ni₇₉Fe₂₁(20 nm)/Ta(5 nm). Such MTJs were fabricated using sputter deposition and patterned using lithographic microfabrication technique followed by optimum heat treatment. Detailed description was reported in previous works by Han *et al.*⁸ We specify excitations for each corresponding peaks in the IET

spectrum. Moreover, we propose a second magnon excitation with $S = 1/2$ and $E_m = 27$ meV which corresponds to the large peak around 20 meV. This excitation corresponds to the Fe spin of the Co₇₅Fe₂₅ electrodes.

We obtain for the tunneling current $I^\gamma = I_0^\gamma + I_p^\gamma + I_{m,i}^\gamma$ where I_0^γ is the elastic tunneling current, I_p^γ denotes the inelastic phonon-assisted tunneling current, and $I_{m,i}^\gamma$ represents the inelastic magnon-assisted tunneling current with $i = 1, 2$ standing for the index of the branch of

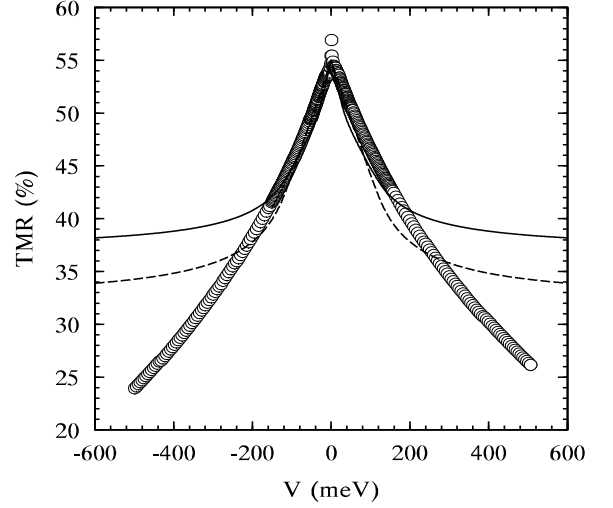


FIG. 3: TMR versus bias voltage at $T = 4.2$ K. Open circles: Experimental data; Solid curve: Calculated TMR of double-magnon and single-phonon assisted tunneling; Dashed curve: Calculated TMR of single-magnon and single-phonon assisted tunneling.

magnon. γ here represents P and AP. These currents are given respectively by $I_0^\gamma = \frac{4\pi e^2 V}{\hbar} [|T^d|^2 + 2(S_1 + S_2)|T^J|^2] A^\gamma$, with T^d and T^J representing direct and spin-dependent charge transfer matrix elements between electrodes.

$$I_p^\gamma = \begin{cases} \frac{e^2 C V}{\hbar} \frac{A^\gamma}{v^4} [(k_B T)^4 \frac{4\pi^4}{15} + \frac{e^4 V^4}{10}], & eV < \omega_D \\ \frac{e^2 C V}{\hbar} \frac{A^\gamma}{v^4} [(k_B T)^4 \frac{4\pi^4}{15} + \omega_D^4 (\frac{1}{2} - \frac{2\omega_D}{5eV})], & eV \geq \omega_D \end{cases} \quad (1)$$

Here C is a constant from the matrix element of electron-phonon interaction. ω_D is the Debye frequency.

$$I_{m,i}^\gamma = \begin{cases} \frac{8\pi e S_i}{\hbar E_{m,i}} |T^J|^2 B^\gamma \left\{ [\frac{1}{2} e^2 V^2 - eV E_c^\gamma + \frac{1}{2} (E_c^\gamma)^2] + 2eV k_B T \ln \left(\frac{1 - e^{-E_{im}/k_B T}}{1 - e^{-E_c^\gamma/k_B T}} \right) \right\}, & eV < E_{m,i} \\ \frac{8\pi e S_i}{\hbar E_{m,i}} |T^J|^2 B^\gamma \left\{ [\frac{1}{2} (E_c^\gamma)^2 + eV (E_{m,i} - E_c^\gamma) - \frac{1}{2} E_{m,i}^2] + 2eV k_B T \ln \left(\frac{1 - e^{-E_{im}/k_B T}}{1 - e^{-E_c^\gamma/k_B T}} \right) \right\}, & eV \geq E_{m,i} \end{cases} \quad (2)$$

E_c^γ was first introduced by Zhang *et al.*⁴ to represent the

wavelength cut-off energy of the spin wave and was later

generalized to the anisotropic one by Han *et al.*¹⁰ In Eqs. (1) and (2), $A^P = B^{\text{AP}} = \rho_M^2 + \rho_m^2$ and $A^{\text{AP}} = B^P = 2\rho_M\rho_m$ with ρ_M (ρ_m) being the density of states in the electrodes for itinerant majority (minority) electrons.

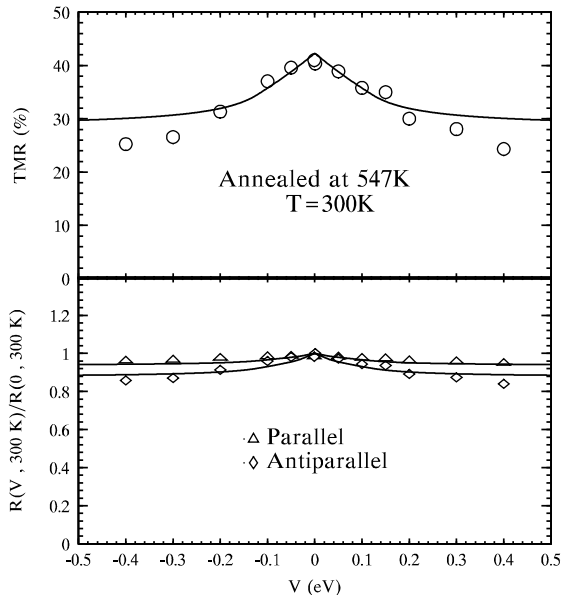


FIG. 4: TMR and R versus bias voltage at $T = 300$ K. Circle: Experimental TMR data; Triangle/Diamond: Experimental resistivity R data for parallel/antiparallel configuration; Solid curves: Theoretical results of single-magnon and single-phonon assisted tunneling.

The main results of our numerical calculation are plotted in Figs. 1 to 6. The parameters used in the calculation are as follows: $R^{\text{AP}}(V = 0) = 171.5 \Omega$, $R^P(V = 0) = 108.1 \Omega$, $\rho_M/\rho_m = 2.83$ and $|T^d|^2/|T^J|^2 = 13.0$. $E_c^{\text{AP}} = 0.104$ meV. $E_c^P = 0.009$ meV. The Debye frequency of Al_2O_3 is taken to be $\omega_D = 84.5$ meV. $e^2C\rho_m^2/(\hbar v^4) = 0.575$. In Fig. 1 IET spectrum via the $S = 3/2$ -magnon-assisted tunneling (dash-dotted curve), $S = 3/2$ -magnon and phonon-assisted tunneling (dashed curve) and double-magnon and single-phonon-assisted tunneling (solid curve) are plotted as functions of voltage V . The experimental data are plotted as crosses in the same figure. From the figure, one clearly sees that the small peak around 115 meV corresponds to the magnon excitation with $S = 3/2$. If one adds phonon excitation on it, one gets the second small peak around 90 meV, which is close to the Debye frequency ω_D . The third strong peak is clearly related to the $S = 1/2$ -magnon excitation. We point out here that as $I_{m,i}^\gamma$ is proportional to S_i , therefore, the height of the magnon peaks is closely related to the relative magnitude of spin S_i . For the strong peak, as $E_{m,i}$ is very small, only $S_i = 1/2$ gives the right relative height corresponding to the one of $S = 3/2$ -magnon.

In order to check if the introduction of the second

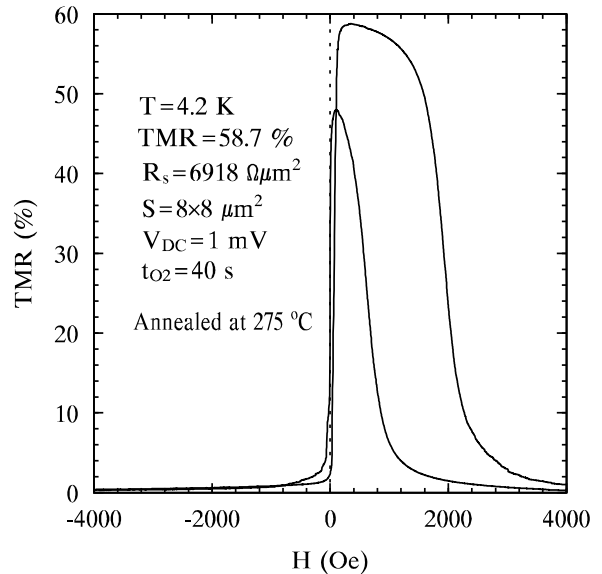


FIG. 5: TMR versus external magnetic field H .

magnon excitation is still consistent with all the measurements, we plot in Figs. 2 and 3 the tunnel current I , the dynamic conductance dI/dV and TMR as functions of voltage V at $T = 4.2$ K for case (i) with all excitations and case (ii) with only $S = 3/2$ -magnon and phonon excitations. It is interesting to see from the figures that the inclusion of the second magnon excitation well represents the experimental results. It is noted that for high voltage, the theoretical results deviate from the experimental data. This is understood that for high voltages, the multi-magnon process becomes important which nevertheless does not included in the present theory.

From $E_{m,i}^\gamma = 3k_B T_c^i / (S_i + 1)$, one has $T_c^1 = 156$ K for $S_1 = 1/2$ magnon. This is reasonable as the concentration of Fe in the electrode is very small and hence the exchange interaction between electron spins of iron is much weaker than the bulk value. Therefore, T_c^1 becomes much smaller than the bulk value. Consequently, we predict that the strong magnon excitation can only be seen at low temperature.

In Fig. 4 we compare our theoretical results of TMR and resistance R versus bias voltage for high temperature $T = 300$ K. As $T > T_c^1$, one only need to consider the single magnon excitation of $S_2 = 3/2$ and the phonon excitation. From the figure one finds the theory fits pretty well with the experimental data.

Finally we discuss the temperature dependence of the TMR. As an example, Fig.5 shows the TMR curves measured at 4.2 K for the same junction after annealing at 548 K for one hour. The junction area is $8 \times 8 \mu\text{m}^2$. A high TMR ratio of 58.7% was observed at 4.2 K, which was much higher than the 41%-room temperature TMR ratio mainly due to the decrease of magnon excitations as

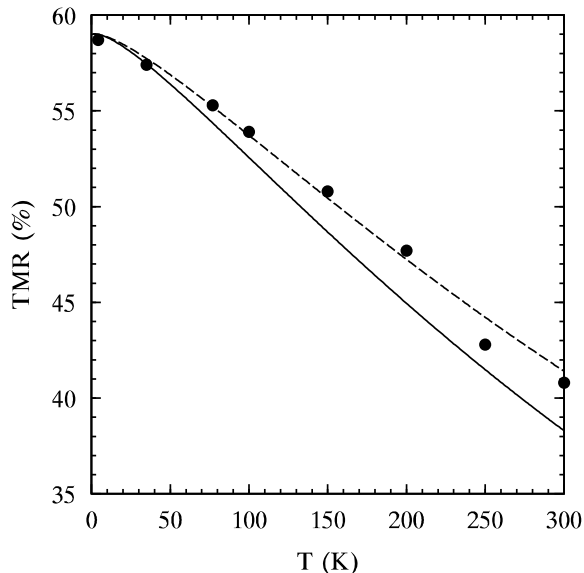


FIG. 6: TMR versus temperature T . Dots: Experimental data; Solid curve: Calculated TMR of double-magnon and single-phonon assisted tunneling; Dashed curve: Calculated TMR of single-magnon and single-phonon assisted tunneling.

well as the absence of phonon excitations. In Fig. 6, TMR is measured from ~ 0 K to 300 K as dots. We plot our theoretical results in the same figure for the cases of double magnon excitation (solid curve) and single magnon excitation (dashed curve). Phonon excitation is included in both curves. As now the temperature crosses the

Curie temperature T_c^1 for $S_1 = 1/2$ -magnon excitation, for $T > T_c^1$, only the branch of $S = 3/2$ -magnon participates in the TMR. Moreover, it is understood that the spin-wave theory is good only for temperature far away from the transition temperature. It is seen from the figure that the solid curve fits the experimental data only at low temperatures. For high temperatures, the dashed curve fits better with the experimental results.

In conclusion, we performed a joint experimental and theoretical investigation of the magnetoelectric properties of the spin-valve-type tunnel junction of Ta(5 nm)/Ni₇₉Fe₂₁ (25 nm)/Ir₂₂Mn₇₈ (10 nm)/Co₇₅Fe₂₅ (4 nm)/Al (0.8 nm)-oxide/Co₇₅Fe₂₅ (4 nm)/Ni₇₉Fe₂₁ (20 nm)/Ta (5 nm). We show that both magnon and phonon excitations contribute to the tunneling process. We further point out that there are two branches of magnon with spin $S = 1/2$ and $3/2$ respectively for the MTJ using Co_{1-x}Fe_x electrodes or using Co/Al-oxide/Fe three key layers. The theory well interpretes the experimental data.

MWW and XFH gratefully acknowledge financial support by the “100 Person Project” of Chinese Academy of Sciences. MWW is also partially supported by Natural Science Foundation of China under Grant No. 10247002. He would also like to thank S. T. Chui at Bartol Research Institute, University of Delaware for hospitality. XFH thanks support from Natural Science Foundation of China under Grant No. 10274103 and the partial support of the State Key Project of Fundamental Research with Grant No. 2001CB610601 of Ministry of Science and technology. CL would like to thank M. Q. Weng for valuable discussion.

* Author to whom correspondence should be addressed; Electronic address: mwwu@ustc.edu.cn

† Mailing Address.

¹ M. Jullière, Phys. Lett. **54A**, 225 (1975).

² T. Miyazaki and N. Tezuka, J. Magn. Magn. Mater. **139**, L231 (1995).

³ J. S. Moodera, L. R. Kinder, T. M. Wong, and R. Meservey, Phys. Rev. Lett. **74**, 3273 (1995).

⁴ S. Zhang, P. M. Levy, A. C. Marley, and S. S. P. Parkin, Phys. Rev. Lett. **79**, 3744 (1997).

⁵ S. T. Chui, Phys. Rev. B **74**, 5600 (1997).

⁶ A. M. Bratkovsky, Appl. Phys. Lett. **72**, 2334 (1998).

⁷ J. M. Daughton, J. Appl. Phys. **81**, 3758 (1997).

⁸ X. F. Han, M. Oogane, H. Kubota, Y. Ando, and T. Miyazaki, Appl. Phys. Lett. **77**, 283 (2000).

⁹ X. F. Han, J. Murai, Y. Ando, H. Kubota, and T. Miyazaki, Appl. Phys. Lett. **78**, 2533 (2001).

¹⁰ X. F. Han, A. C. C. Yu, M. Oogane, J. Murai, T. Daibou, and T. Miyazaki, Phys. Rev. B **63**, 224404 (2001).

¹¹ M. Sato and K. Kobayashi, IEEE Trans. Magn. **33**, 3553 (1997).

¹² K. Tsukagoshi, B. W. Alphenaar, and H. Ago, Nature (London) **401**, 572 (1999).

¹³ S. Tehrani, J.M. Slaughter, E. Chen, M. Durlam, J. Shi, and M. DeHerrera, IEEE. Trans. Mags. **35**, 2814 (2000).

¹⁴ K. Machida, N. Hayashi, Y. Miyamoto, T. Tamaki, and H. Okuda, J. Magn. Magn. Mater. **235**, 201 (2001).

¹⁵ A. M. Bratkovsky, Phys. Rev. B **56**, 2344 (1997).